中国激光

实现正交偏振嵌位的受激布里渊随机光纤激光器

宁金星[1,2]，王春华[1,2*]，方捻[1,2]，谷祥[1,2]，吴科帅[1,2]

[1]上海大学通信与信息工程学院，上海 200444；

[2]特种光纤与光接入网重点实验室，上海 200444

摘要 布里渊随机光纤激光器(BRFL)是基于受激布里渊散射(SBS)效应和随机分布式反馈谐振腔组成的新型激光器。笔者基于保偏光纤(PMF)中SBS的非线性轴向偏振牵引效应，提出并实现了一种可实现正交偏振嵌位的受激布里渊随机光纤激光器(PMF-BRFL)。首先对PMF-BRFL系统的偏振工作分区进行了理论分析，接着讨论了系统偏振嵌位的动态范围与系统参数之间的关系，最后采用3 km长PMF实现了PMF-BRFL系统。该系统可以实现偏振态稳定正交嵌位的窄带激光输出，实验结果与理论分析结果一致。

关键词 激光器；受激布里渊散射；随机光纤激光器；偏振牵引效应；正交偏振嵌位；保偏光纤

中图分类号 O436 **文献标志码** A **DOI**：10.3788/CJL220839

1 引 言

光纤中的受激布里渊散射(SBS)是光纤中相向传播的泵浦光与泵浦激发产生的信号光之间相互作用的非线性光学效应，具有低阈值、超窄线宽、增益效率高、对外界环境(温度、应力等)敏感等特性，目前已被广泛应用于布里渊放大器[1-3]、布里渊滤波器[4-7]、布里渊光时域分析仪[8-11]以及布里渊光纤陀螺[12-14]。随机光纤激光器[15-16]主要是基于光纤的增益效应，包括稀土掺杂(EDFA)、受激拉曼增益及SBS增益等，结合光纤瑞利散射或人工制备的随机散射器件(如随机光纤光栅)实现的随机激光腔构建而成的。SBS的超窄增益带宽可以实现低强度噪声、低相位噪声、窄线宽单频激光输出，在构建光纤随机激光器上具有天然优势。基于高阶效应，SBS还可以实现100多个波长的多波长随机激光器[17]。然而，迄今为止关于布里渊随机激光器(BRFL)的研究主要集中在非偏振参数(如激光功率、强度相位噪声、线宽等)上[18-23]，而对其偏振特性的研究还未见公开报道。

单模光纤(SMF)中存在由制备及盘绕引入的应力以及结构各向异性导致的随机双折射[24-25]，因而其SBS效应具有偏振随机性，SBS增益、布里渊频移等都与偏振相关。一直以来，人们针对SBS的增益偏振相关性以及如何消除其影响进行了大量研究[26-30]，而对光纤SBS偏振效应本身的研究则始于2008年，当时，Zadok等[31]通过理论分析提出了单模光纤中SBS的偏振牵引现象，并通过实验进行了验证。在理想的SMF中，SBS偏振牵引主要表现为信号光偏振态(SOP)会受到相向传输的泵浦光偏振态的牵引，并向入射泵浦偏振态的方向靠近。然而，实际的SMF中存在着不可避免的随机双折射，信号光偏振态不仅受SBS效应中泵浦光偏振态的牵引，还受光纤随机双折射的影响，导致信号光偏振态的被牵引方向不确定。理论研究发现，在实际的SMF中，信号光偏振态的整体牵引方向由入射泵浦光偏振态和光纤双折射共同决定，并向使信号光SBS增益最大的偏振方向演进[32]。进一步，人们又发现在保偏光纤(PMF)中，SBS具有轴向偏振牵引效应，即信号光偏振态总是被牵引向入射泵浦光偏振态靠近的PMF主轴方向[33]。

基于PMF的SBS轴向偏振牵引效应，本团队提出并实现了一种基于PMF的线腔布里渊随机光纤激光器(PMF-BRFL)，它可以对任意偏振态泵浦光实现正交偏振嵌位整形的激光输出，即：对任意入射泵浦光偏振态，PMF-BRFL可以实现输出偏振态总被锁定于PMF主轴对应的两正交偏振态之一。笔者对PMF-BRFL系统偏振工作状态的划分进行了理论分析和实验研究，分析了入射泵浦光偏振态和泵浦功率对系统输出偏振态和输出功率的影响，并对输出激光的线宽和光谱特性进行了测量。

2 PMF-BRFL理论模型与分析

在图1所示的线腔PMF-BRFL中，PMF既构成了线形随机激光腔，同时又为激光器提供SBS增益。泵浦光在沿PMF传播过程中首先产生反向的自发辐射

收稿日期：2022-05-10；**修回日期**：2022-06-16；**录用日期**：2022-08-18；**网络首发日期**：2022-08-28

基金项目：国家自然科学基金面上项目(61575118，62075123)

通信作者：*lizawch@staff.shu.edu.cn

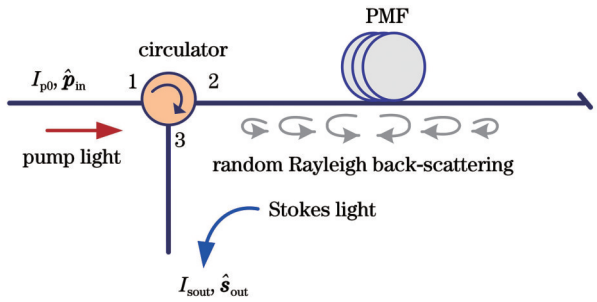

图 1　线腔 PMF-BRFL 光路

Fig. 1　Diagram of line-cavity PMF-BRFL

Stokes 信号光，该信号光反向传播，受 SBS 增益放大。反向传播的 Stokes 光在传播过程中产生同频的一次瑞利背向散射，进而产生与 Stokes 光同向的二次瑞利散射，二次瑞利散射受到 SBS 增益而放大，由此构建起在 PMF 中的随机激光腔。当泵浦光功率超过随机腔的激光发射阈值时，输出随机激光，并由环形器的端口 3 输出。

在 PMF 中，若忽略泵浦耗尽，即不计入射泵浦功率 I_{p0} 在传播过程中的衰耗，SBS 效应中的信号光功率 I_s 和偏振态 $\hat{\boldsymbol{s}}=(s_1,s_2,s_3)$ 的传播方程[32-33]可以分别表示为

$$\frac{\mathrm{d}I_s}{\mathrm{d}z}=g_0 I_{p0} I_s\left[1+(\hat{\boldsymbol{p}}_{in}\cdot\hat{\boldsymbol{\beta}}_1)(\hat{\boldsymbol{s}}\cdot\hat{\boldsymbol{\beta}}_1)\right], \tag{1}$$

$$\frac{\mathrm{d}\left(\hat{\boldsymbol{s}}\cdot\hat{\boldsymbol{\beta}}_1\right)}{\mathrm{d}z}=g_0 I_{p_0}\hat{\boldsymbol{p}}_{in}\cdot\hat{\boldsymbol{\beta}}_1\left[1-\left(\hat{\boldsymbol{s}}\cdot\hat{\boldsymbol{\beta}}_1\right)^2\right], \tag{2}$$

式中：g_0 为 SBS 的增益系数；$\hat{\boldsymbol{p}}_{in}$ 为入射泵浦光偏振态；$\hat{\boldsymbol{\beta}}_1$ 位于邦加球的赤道平面上，为 $\boldsymbol{\beta}_1$ 的归一化单位矢量，$\boldsymbol{\beta}_1=(\beta_1,\beta_2,0)=2\pi_1/\left(L_b\hat{\boldsymbol{\beta}}_1\right)$ 为 PMF 的偏振矢量，其中 L_b 为保偏光纤拍长。式(1)描述了传播过程中信号光强的变化。式(2)描述了信号光偏振态 $\hat{\boldsymbol{s}}$ 被牵引向 $\mathrm{sign}\left[(\hat{\boldsymbol{p}}_{in}\cdot\hat{\boldsymbol{\beta}}_1)\hat{\boldsymbol{\beta}}_1\right]$，即 PMF 的两个主轴之一($\hat{\boldsymbol{\beta}}_1$ 或 $-\hat{\boldsymbol{\beta}}_1$)，其中：牵引方向取决于 $\hat{\boldsymbol{p}}_{in}\cdot\hat{\boldsymbol{\beta}}_1$ 的符号；牵引力的大小为 $g_0 I_{p_0}\hat{\boldsymbol{p}}_{in}\cdot\hat{\boldsymbol{\beta}}_1$，与 g_0、I_{p0} 以及 $\hat{\boldsymbol{p}}_{in}$ 与 PMF 主轴的相对位置 $\hat{\boldsymbol{p}}_{in}\cdot\hat{\boldsymbol{\beta}}_1$ 的大小成正比。当泵浦光偏振态在 $\hat{\boldsymbol{p}}_{in}\cdot\hat{\boldsymbol{\beta}}_1>0$ 或 $\hat{\boldsymbol{p}}_{in}\cdot\hat{\boldsymbol{\beta}}_1<0$ 两种状态之间变化时，信号光偏振态 $\hat{\boldsymbol{s}}$ 的被牵引方向在 $\hat{\boldsymbol{\beta}}_1$ 和 $-\hat{\boldsymbol{\beta}}_1$ 之间变更。而当 $\hat{\boldsymbol{p}}_{in}\cdot\hat{\boldsymbol{\beta}}_1=0$ 时，SBS 的牵引力为 0，此时 $\hat{\boldsymbol{s}}$ 不受 SBS 非线性偏振牵引的影响，仅受 PMF 的线双折射作用，且传播过程中仅围绕 $\hat{\boldsymbol{\beta}}_1$ 旋转，而非向着 $\pm\hat{\boldsymbol{\beta}}_1$ 方向演进。

由式(1)和式(2)可以得到 PMF 中信号光的 SBS 增益的解析解为

$$G=\frac{1}{2}\left[\left(1+\hat{\boldsymbol{s}}_{in}\cdot\hat{\boldsymbol{\beta}}_1\right)\exp\left(g_0 I_{p0}\hat{\boldsymbol{p}}_{in}\cdot\hat{\boldsymbol{\beta}}_1 L\right)+\left(1-\hat{\boldsymbol{s}}_{in}\cdot\hat{\boldsymbol{\beta}}_1\right)\cdot\exp\left(-g_0 I_{p0}\hat{\boldsymbol{p}}_{in}\cdot\hat{\boldsymbol{\beta}}_1 L\right)\right]\exp\left(g_0 I_{p0}L\right), \tag{3}$$

式中：L 为 PMF 长度。可见，在忽略泵浦耗尽的情况下，PMF 光纤中的 SBS 增益除了与入射泵浦光功率直接相关外，还与入射泵浦光和信号光的偏振态有关，但不是直接由入射泵浦光、信号光偏振态的确切位置决定，而是由其与 PMF 主轴的相对位置(即 $\hat{\boldsymbol{p}}_{in}\cdot\hat{\boldsymbol{\beta}}_1$ 和 $\hat{\boldsymbol{s}}_{in}\cdot\hat{\boldsymbol{\beta}}_1$)决定的。

在特殊情况下，当 $\hat{\boldsymbol{s}}_{in}\cdot\hat{\boldsymbol{\beta}}_1=\pm1$ 时，即入射信号光偏振态沿 PMF 主轴进入光纤时，信号光将经历最大或者最小 SBS 增益：

$$G_{\beta/-\beta}(\hat{\boldsymbol{p}}_{in}\cdot\hat{\boldsymbol{\beta}}_1)=\exp\left[g_0 I_{p0}L(1\pm\hat{\boldsymbol{p}}_{in}\cdot\hat{\boldsymbol{\beta}}_1)\right]。 \tag{4}$$

图 2(a)给出了 PMF 中 SBS 增益与 $\hat{\boldsymbol{p}}_{in}\cdot\hat{\boldsymbol{\beta}}_1$、$\hat{\boldsymbol{s}}_{in}\cdot\hat{\boldsymbol{\beta}}_1$ 理论关系的三维图。仿真中，PMF 长度 $L=3$ km，入射泵浦功率 $I_{p0}=5$ mW，SBS 增益系数 $g_0=0.1229\ \mathrm{km^{-1}\cdot mW^{-1}}$。图 2(b)给出了 $\hat{\boldsymbol{s}}_{in}\cdot\hat{\boldsymbol{\beta}}_1$ 取值不同时，SBS 增益与 $\hat{\boldsymbol{p}}_{in}\cdot\hat{\boldsymbol{\beta}}_1$ 的关系。可见：当 $\hat{\boldsymbol{s}}_{in}\cdot\hat{\boldsymbol{\beta}}_1=\pm1$ 时，即入射信号光沿 PMF 主轴进入光纤时，随着泵浦偏振态 $\hat{\boldsymbol{p}}_{in}\cdot\hat{\boldsymbol{\beta}}_1$ 变化，SBS 增益的变化最大。当 $\hat{\boldsymbol{p}}_{in}\cdot\hat{\boldsymbol{\beta}}_1=1$ 时，$\hat{\boldsymbol{\beta}}_1$ 偏振的信号光增益最大，$-\hat{\boldsymbol{\beta}}_1$ 偏振的信号光增益为零，反之亦反；当 $\hat{\boldsymbol{p}}_{in}\cdot\hat{\boldsymbol{\beta}}_1=0$ 时，$\pm\hat{\boldsymbol{\beta}}_1$ 偏振的信号光的 SBS 增益相同。

在图 1 所示的由 PMF 构建的随机谐振腔中，$\pm\hat{\boldsymbol{\beta}}_1$ 偏振模式具有最大的 SBS 增益，根据模式竞争原则，相对于其他偏振模式，这两种相互正交的偏振模式可以胜出并维持振荡。假设信号光在传播过程中经历一次和二次瑞利随机分布散射后的等效瑞利反射系数为 R，光纤的传输损耗系数为 α，则可以得到激光起振的阈值方程为

$$R\exp(-2\alpha L)\exp\left[g_0 I_{p0th}L\left(1\pm\hat{\boldsymbol{p}}_{in}\cdot\hat{\boldsymbol{\beta}}_1\right)\right]=1, \tag{5}$$

式中："±"对应 $\pm\hat{\boldsymbol{\beta}}_1$ 偏振模式。故而，PMF-BRFL 中的 $\pm\hat{\boldsymbol{\beta}}_1$ 激光模式的阈值功率为

$$I_{p0th,\pm\beta}=\frac{2\alpha L-\ln R}{\left(1\pm\hat{\boldsymbol{p}}_{in}\cdot\hat{\boldsymbol{\beta}}_1\right)g_0 L}\triangleq\frac{I_{p0th}}{1\pm\hat{\boldsymbol{p}}_{in}\cdot\hat{\boldsymbol{\beta}}_1}。 \tag{6}$$

可见，$\pm\hat{\boldsymbol{\beta}}_1$ 偏振模式的起振阈值与入射泵浦偏振 $\hat{\boldsymbol{p}}_{in}\cdot\hat{\boldsymbol{\beta}}_1$ 直接相关，在 $|\hat{\boldsymbol{p}}_{in}\cdot\hat{\boldsymbol{\beta}}_1|\neq0$ 时有着不同的起振阈值，阈值低的偏振模式优先起振。图 2(c)给出了 PMF 长度 $L=3$ km，$\alpha=0.3$ dB/km，等效瑞利反射系数 $R=10^{-5}$ 时，由 $I_{p0th,\pm\beta}$ 在泵浦功率和 $\hat{\boldsymbol{p}}_{in}\cdot\hat{\boldsymbol{\beta}}_1$ 二维平面分割的 4 个工作区间。这 4 个工作区间分别为：1)$\hat{\boldsymbol{\beta}}_1$ 模式工作区间，满足 $I_{p0th,\beta}\leqslant I_{p0}\leqslant I_{p0th,-\beta}$，此时只有 $\hat{\boldsymbol{\beta}}_1$ 模式的激光输出；2)$-\hat{\boldsymbol{\beta}}_1$ 模式工作区间，满足 $I_{p0th,-\beta}\leqslant I_{p0}\leqslant I_{p0th,\beta}$，此时只有 $-\hat{\boldsymbol{\beta}}_1$ 模式的激光输出；3)$\pm\hat{\boldsymbol{\beta}}_1$ 偏振模式同时振荡的退偏区，此时同时满足 $I_{p0}\geqslant I_{p0th,\pm\beta}$；4)自发辐射区间，此时同时满足 $I_{p0}<I_{p0th,\pm\beta}$，PMF-BRFL 没有激光输出，而是输出自发辐射光。由此可以推导出 $\pm\hat{\boldsymbol{\beta}}_1$ 模式同时激射时的退偏区宽度为

$$W=2\left(\frac{2\alpha L-\ln R}{I_{p0}g_0 L}-1\right)。 \tag{7}$$

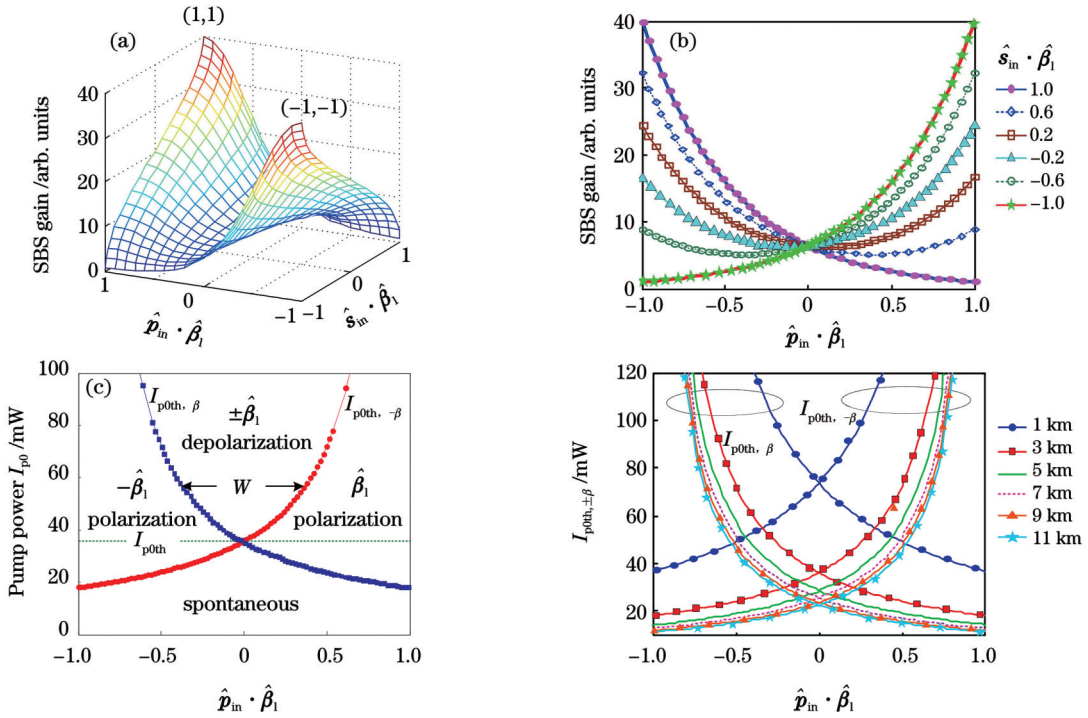

图 2　PMF-BRFL 中 SBS 增益与偏振工作区间的理论关系。(a) PMF 中 SBS 增益与 $\hat{\boldsymbol{p}}_{in}\cdot\hat{\boldsymbol{\beta}}_1$、$\hat{\boldsymbol{s}}_{in}\cdot\hat{\boldsymbol{\beta}}_1$ 的三维关系图；(b)不同 $\hat{\boldsymbol{s}}_{in}\cdot\hat{\boldsymbol{\beta}}_1$ 取值下，SBS 增益与 $\hat{\boldsymbol{p}}_{in}\cdot\hat{\boldsymbol{\beta}}_1$ 的关系；(c)PMF 长度 L=3 km 时，由 $I_{p0th,\pm\beta}$ 划分的 PMF-BRFL 偏振工作区间；(d)不同 PMF 长度时的 $I_{p0th,\pm\beta}$ 曲线

Fig. 2　Theoretical relationship between SBS gain and polarization operating range in PMF-BRFL. (a) Three-dimensional relationship diagram of SBS gain with $\hat{\boldsymbol{p}}_{in}\cdot\hat{\boldsymbol{\beta}}_1$ and $\hat{\boldsymbol{s}}_{in}\cdot\hat{\boldsymbol{\beta}}_1$ in PMF; (b) relationship between SBS gain and $\hat{\boldsymbol{p}}_{in}\cdot\hat{\boldsymbol{\beta}}_1$ for different $\hat{\boldsymbol{s}}_{in}\cdot\hat{\boldsymbol{\beta}}_1$ cases; (c) PMF-BRFL polarization working ranges divided by $I_{p0th,\pm\beta}$, as PMF length L=3 km; (d) $I_{p0th,\pm\beta}$ curves for different PMF lengths

当 $I_{p0}=I_{p0th}$ 时，W=0，此时 PMF-BRFL 具有最大的偏振嵌位工作范围，系统对除 $\hat{\boldsymbol{p}}_{in}\cdot\hat{\boldsymbol{\beta}}_1=0$ 以外的所有泵浦偏振态都有偏振嵌位作用。图 2(d)给出了不同 PMF 长度时 $I_{p0th,\pm\beta}$ 与 $\hat{\boldsymbol{p}}_{in}\cdot\hat{\boldsymbol{\beta}}_1$ 的关系曲线，可见：当 PMF 较短(1～3 km)时，阈值从 75 mW 下降到 38 mW，下降得较快；当 PMF 长度超过 3 km 后，阈值下降得比较慢。因此，对于建立的 PMF-BRFL 系统来说，3～5 km 的 PMF 随机腔长即可实现较高的泵浦效率。

3　PMF-BRFL 系统的正交偏振嵌位

采用长度为 3 km 的 PMF 搭建了如图 3 所示的 PMF-BRFL 实验系统。

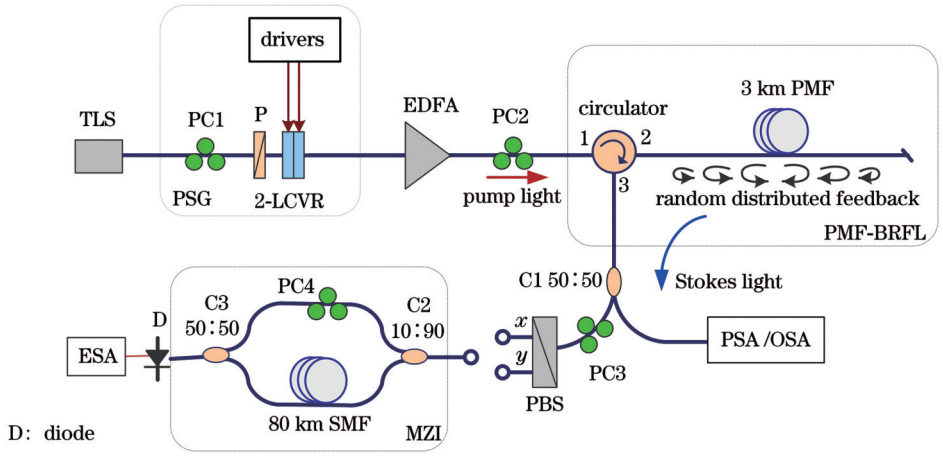

图 3　PMF-BRFL 实验系统图

Fig. 3　Diagram of PMF-BRFL experimental system

系统中可调谐激光器(Santec MLS800)输出中心波长为 1553.73 nm 的泵浦光，泵浦光进入偏振发生器(PSG)，PSG 由偏振控制器 1(PC1)、起偏器(P)、两个液晶相位可变延迟器(LCVR)构成。改变 LCVR 的驱

动电压可以实现任意偏振态的泵浦输出光。PSG输出的泵浦光经掺铒光纤放大器(EDFA)放大后，由偏振控制器PC2调节初始偏振态 $\hat{\boldsymbol{p}}_{\mathrm{in}}$ 与PMF主轴的相对位置，经环形器的端口1送入3 km PMF。激光输出由耦合器C1分路后，分别采用偏振分析仪(PSA)、光谱仪(OSA)和频谱仪(ESA)对其偏振态、光强、光谱、线宽等特性进行测量。

设置LCVR的驱动电压，在邦加球的大圆上随机生成100个输入泵浦光偏振态 $\hat{\boldsymbol{p}}_{\mathrm{in}}$，如图4(a)所示。设置EDFA的输出功率为 $I_{\mathrm{p0\_edfa}}=55$ mW，调节PC2，待PMF-BRFL的激光输出取得最大值时，将第一个泵浦偏振态 $\hat{\boldsymbol{p}}_{\mathrm{in}}^{\#1}$ 调节到与PMF的主轴对准，此时 $\left|\hat{\boldsymbol{p}}_{\mathrm{in}}\cdot\hat{\boldsymbol{\beta}}_1\right|=1$。图4(c)是与 $\hat{\boldsymbol{p}}_{\mathrm{in}}^{\#100}$ 对应的 $\hat{\boldsymbol{p}}_{\mathrm{in}}\cdot\hat{\boldsymbol{\beta}}_1=\hat{\boldsymbol{p}}_{\mathrm{in}}\cdot\hat{\boldsymbol{p}}_{\mathrm{in}}^{\#1}$ 的分布。图4(b)是与 $\hat{\boldsymbol{p}}_{\mathrm{in}}^{\#100}$ 对应的输出的随机激光偏振态 $\hat{\boldsymbol{s}}_{\mathrm{out}}$ 在邦加球上的分布，可见：与 $\hat{\boldsymbol{p}}_{\mathrm{in}}^{\#100}$ 相比，输出激光偏振态绝大部分被嵌位于 $\pm\hat{\boldsymbol{\beta}}_1$，只有几个点落入邦加球内。图4(d)为测量得到的对应 $\hat{\boldsymbol{p}}_{\mathrm{in}}^{\#100}$ 的 $\hat{\boldsymbol{s}}_{\mathrm{out}}\cdot\hat{\boldsymbol{\beta}}_1$ 的变化，可见：在PMF-BRFL中，对于任意随机分布的 $\hat{\boldsymbol{p}}_{\mathrm{in}}$，输出激光偏振态绝大多数被嵌位于 $\mathrm{sign}(\hat{\boldsymbol{p}}_{\mathrm{in}}\cdot\hat{\boldsymbol{\beta}}_1)\hat{\boldsymbol{\beta}}_1$。由图4(e)给出的 $\hat{\boldsymbol{s}}_{\mathrm{out}}\cdot\hat{\boldsymbol{\beta}}_1$ 与 $\hat{\boldsymbol{p}}_{\mathrm{in}}\cdot\hat{\boldsymbol{\beta}}_1$ 的测量关系可以看出：在 $\hat{\boldsymbol{p}}_{\mathrm{in}}\cdot\hat{\boldsymbol{\beta}}_1\in(-0.1,0.1)$ 区间内，激光输出偏振态没有被嵌位至理想的 $\pm\hat{\boldsymbol{\beta}}_1$ 位置。这是因为在 $\hat{\boldsymbol{p}}_{\mathrm{in}}\cdot\hat{\boldsymbol{\beta}}_1=0$ 附近，$\pm\hat{\boldsymbol{\beta}}_1$ 偏振模式的SBS增益相同或相近，系统工作在两个模式同时起振的退偏区。在距离 $\hat{\boldsymbol{p}}_{\mathrm{in}}\cdot\hat{\boldsymbol{\beta}}_1=0$ 稍远的区域，$\pm\hat{\boldsymbol{\beta}}_1$ 两正交偏振模式的增益差异显著，PMF-BRFL振荡在 $\mathrm{sign}(\hat{\boldsymbol{p}}_{\mathrm{in}}\cdot\hat{\boldsymbol{\beta}}_1)\hat{\boldsymbol{\beta}}_1$ 单偏的全偏振区。

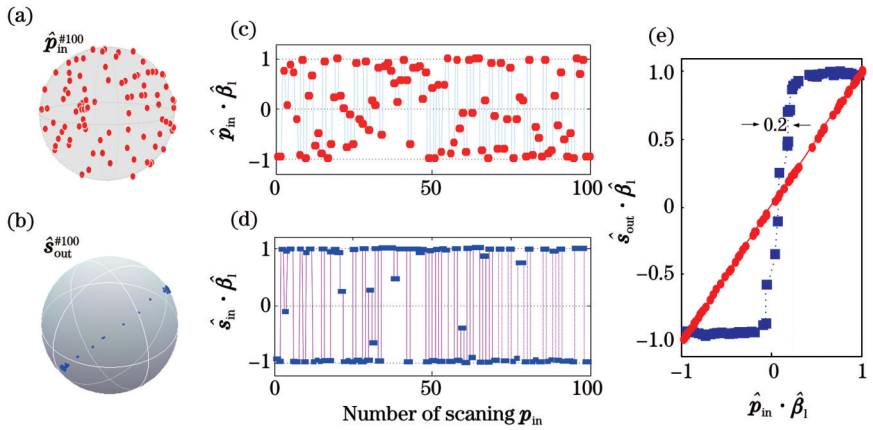

图4　PMF-BRFL实验结果。(a)产生的100个随机分布在邦加球上的输入泵浦光偏振态；(b)对应 $\hat{\boldsymbol{p}}_{\mathrm{in}}^{\#100}$ 的随机激光输出偏振态；(c)与 $\hat{\boldsymbol{p}}_{\mathrm{in}}^{\#100}$ 对应的 $\hat{\boldsymbol{p}}_{\mathrm{in}}\cdot\hat{\boldsymbol{\beta}}_1=\hat{\boldsymbol{p}}_{\mathrm{in}}\cdot\hat{\boldsymbol{p}}_{\mathrm{in}}^{\#1}$ 分布；(d)测量得到的 $\hat{\boldsymbol{s}}_{\mathrm{out}}\cdot\hat{\boldsymbol{\beta}}_1$ 分布；(e)测量的 $\hat{\boldsymbol{s}}_{\mathrm{out}}\cdot\hat{\boldsymbol{\beta}}_1$ 与 $\hat{\boldsymbol{p}}_{\mathrm{in}}\cdot\hat{\boldsymbol{\beta}}_1$ 之间的关系

Fig. 4　PMF-BRFL experimental results. (a) 100 generated SOPs of input pump light randomly distributed in Poincaré sphere; (b) SOPs of random lasing light corresponding to $\hat{\boldsymbol{p}}_{\mathrm{in}}^{\#100}$; (c) $\hat{\boldsymbol{p}}_{\mathrm{in}}\cdot\hat{\boldsymbol{\beta}}_1=\hat{\boldsymbol{p}}_{\mathrm{in}}\cdot\hat{\boldsymbol{p}}_{\mathrm{in}}^{\#1}$ distribution corresponding to $\hat{\boldsymbol{p}}_{\mathrm{in}}^{\#100}$; (d) measured $\hat{\boldsymbol{s}}_{\mathrm{out}}\cdot\hat{\boldsymbol{\beta}}_1$ distribution; (e) relationship between measured $\hat{\boldsymbol{s}}_{\mathrm{out}}\cdot\hat{\boldsymbol{\beta}}_1$ and $\hat{\boldsymbol{p}}_{\mathrm{in}}\cdot\hat{\boldsymbol{\beta}}_1$

针对不同的泵浦功率，设置EDFA的输出功率 $I_{\mathrm{p0\_edfa}}$ 分别为40、50、55、80、120 mW，对PMF-BRFL的输出激光偏振态进行测量，测量结果如图5所示。图5(a)～(e)为输出激光偏振态在邦加球上的变化轨迹；图5(f)～(j)为对应的 $\hat{\boldsymbol{s}}_{\mathrm{out}}\cdot\hat{\boldsymbol{\beta}}_1$ 分布。图5(k)～(o)给出了各泵浦功率下测量得到的输出激光偏振度(DOP)与 $\hat{\boldsymbol{p}}_{\mathrm{in}}\cdot\hat{\boldsymbol{\beta}}_1$ 的关系曲线，可见：PMF-BRFL的退偏区间 W 随着泵浦光功率而改变，即不同泵浦光功率下处于邦加球内的偏振态点数不同：当 $I_{\mathrm{p0\_edfa}}=55$ mW时，球内偏振点数最少，W 最窄，系统偏振嵌位整形的工作范围最大；当 $I_{\mathrm{p0\_edfa}}<55$ mW时，PMF-BRFL在退偏区为自发辐射；当 $I_{\mathrm{p0\_edfa}}>55$ mW时，PMF-BRFL在退偏区为双偏振模激射。

环形器端口1到端口2存在插入损耗，测得实验系统中实际进入PMF的泵浦功率 I_{p0} 与EDFA的输出功率设置 $I_{\mathrm{p0\_edfa}}$ 之间相差1.87 dB。图6(a)给出了在 $I_{\mathrm{p0\_edfa}}$ 为40、50、55、60、80、100、120、150 mW时，退偏区宽度的测量值(蓝点)，以及由式(7)计算得出的 $L=3$ km时退偏区宽度 W 与 I_{p0} 泵浦功率之间的理论关系曲线(红线)。可见，两者具有良好的一致性。

实验中发现，即使在 $I_{\mathrm{p0}}=I_{\mathrm{p0th}}$ 的位置处，系统也难以实现 $W=0$ 的工作点。这是由于虽然SBS具有良好的偏振牵引效应，但PMF随机反射腔中的瑞利散射光并不具备理想的偏振保持能力，也就是说，在光纤随机腔中，瑞利分布散射光的偏振态与瑞利泵浦光(振荡激光)的偏振态并不一致，从而导致 $\pm\hat{\boldsymbol{\beta}}_1$ 模式在两者增益相近区域的模式竞争结果的确定性下降。图6(a)中还给出了其他不同光纤腔长时，退偏区宽度与泵浦功率间的理论关系曲线。可见，虽然短腔长对泵浦功率的要求较高，但其 $W=0$ 工作点附近的退偏区宽度 W 的变化缓慢。图6(b)给出了系统工作要求 $W=0.1$ 和0.2时，泵浦功率的动态范围与PMF腔长的理论关系。可见：相对于长腔长，PMF腔长在1～3 km范围时，针对确定的偏振整形要求，泵浦功率具有较大的动态工作范围。

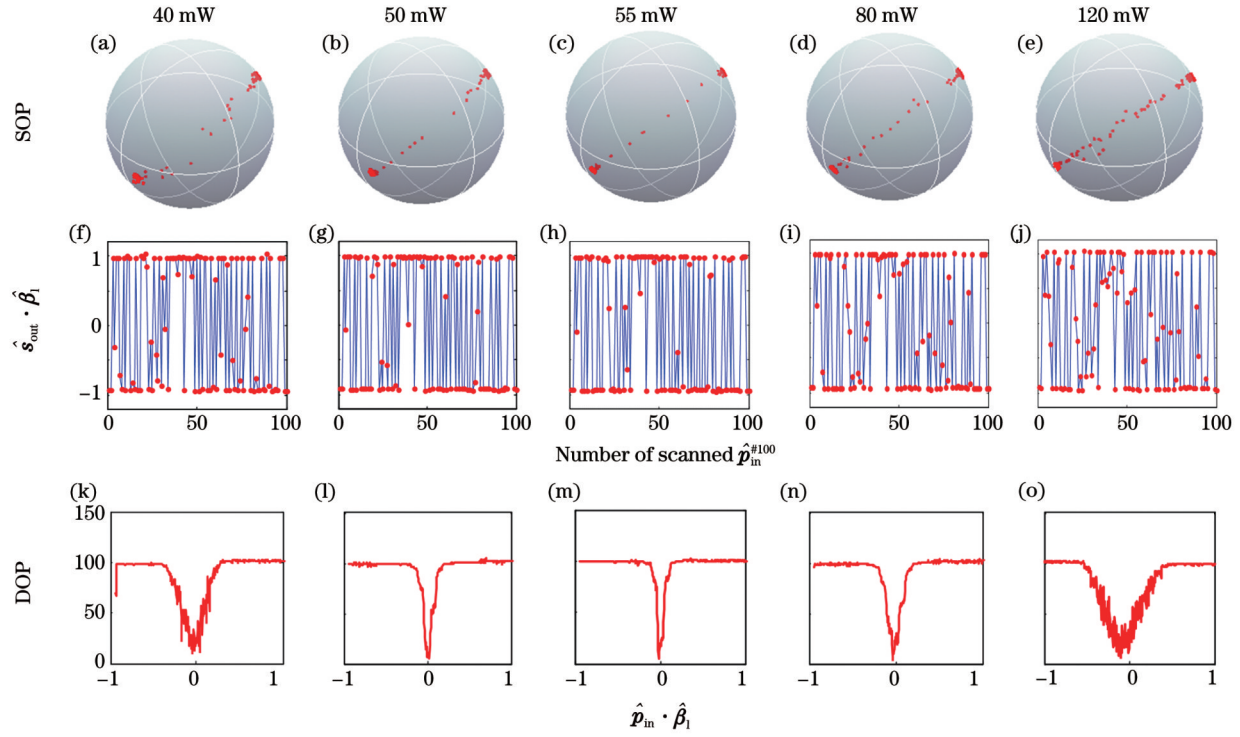

图 5　不同泵浦功率时，对应 $\hat{\boldsymbol{p}}_{\text{in}}^{\#100}$ 的测量结果。(a)～(e)测量得到的 PMF-BRFL 的激光输出偏振态；(f)～(j)$\hat{\boldsymbol{s}}_{\text{out}}\cdot\hat{\boldsymbol{\beta}}_1$ 的分布；(k)～(o)DOP 与 $\hat{\boldsymbol{p}}_{\text{in}}\cdot\hat{\boldsymbol{\beta}}_1$ 的关系

Fig. 5　Measurement results of $\hat{\boldsymbol{p}}_{\text{in}}^{\#100}$ for different pump powers. (a)–(e) Measured SOPs of lasing light of PMF-BRFL; (f)–(j) distribution of $\hat{\boldsymbol{s}}_{\text{out}}\cdot\hat{\boldsymbol{\beta}}_1$; (k)–(o) relationship of DOP versus $\hat{\boldsymbol{p}}_{\text{in}}\cdot\hat{\boldsymbol{\beta}}_1$

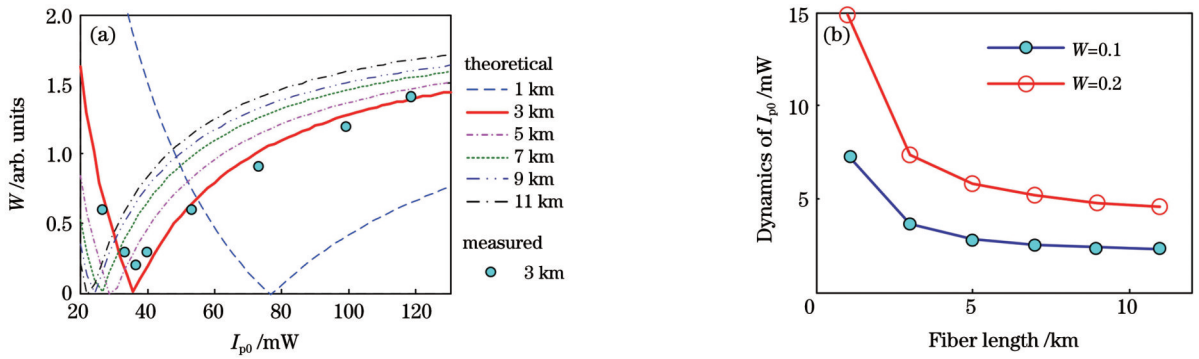

图 6　退偏区宽度-泵浦功率以及泵浦功率动态范围-腔长的理论关系。(a)不同 PMF 腔长时，退偏区宽度 W 与泵浦功率 I_{p0} 之间的理论关系(线)以及 L=3 km 时实验测得的 W 与泵浦功率 I_{p0} 的关系(点)；(b)不同退偏区宽度要求下，系统泵浦功率的动态范围与 PMF 腔长之间的理论关系

Fig. 6　Theoretical relationship between depolarization domain width and pump power, as well as working dynamics of pump power and cavity length. (a) Theoretical relationship (lines) between depolarization region width W and pump power I_{p0} for different PMF cavity lengths, and measured relationship between depolarization region width W and pump power I_{p0} (dots) in the case of L=3 km; (b) theoretical relationships between working dynamics of pump power and cavity length of PMF for different W-requirements

接下来，本课题组对 PMF-BRFL 系统的激光输出功率特性进行了测试。图 7(a)给出了不同 EDFA 输出功率下，由 PSA 检测的系统激光输出功率与泵浦偏振态 $\hat{\boldsymbol{p}}_{\text{in}}\cdot\hat{\boldsymbol{\beta}}_1$ 之间的关系。可见，PMF-BRFL 输出激光功率随 $\hat{\boldsymbol{p}}_{\text{in}}\cdot\hat{\boldsymbol{\beta}}_1$ 的不同而不同。图 7(b)给出了 $I_{\text{p0\_edfa}}$=55 mW 时，不同泵浦偏振态 $\hat{\boldsymbol{p}}_{\text{in}}\cdot\hat{\boldsymbol{\beta}}_1$ 设置下，由 OSA 测得的系统激光输出光谱。插图中给出了 $\hat{\boldsymbol{p}}_{\text{in}}\cdot\hat{\boldsymbol{\beta}}_1$=0 和 $\hat{\boldsymbol{p}}_{\text{in}}\cdot\hat{\boldsymbol{\beta}}_1$=1 时的测量光谱，两者功率相差约 15 dBm。在光谱中可以看到泵浦光的瑞利散射边峰与激光输出波长相差一个布里渊频移 0.088 nm，幅度相差约 50 dBm。

接下来，本课题组用图 3 所示的 C2、C3、PC4 和 80 km SMF 构成 Mach-Zehnder 干涉结构(MZI)，用频谱仪检测 MZI 中两路干涉光的干涉频谱，对 PMF-BRFL 的输出激光线宽进行测量。在测试中，首先利

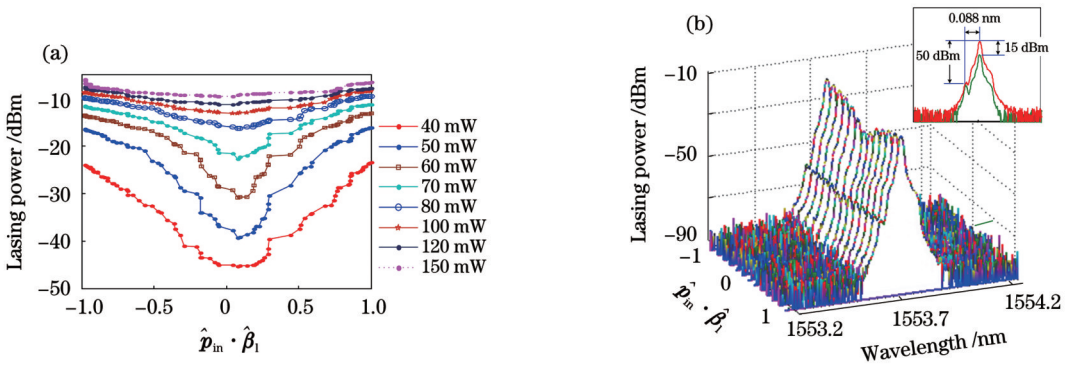

图 7　不同 I_{p0_edfa} 时测量得到的系统激光输出特性。(a)随机激光输出功率与泵浦偏振态 $\hat{\boldsymbol{p}}_{in}\cdot\hat{\boldsymbol{\beta}}_1$ 之间的关系；(b)系统激光输出光谱

Fig. 7　Laser output characteristics of the system under different setting values of I_{p0_edfa}. (a) Relationship between output power of lasing light and pump polarization state $\hat{\boldsymbol{p}}_{in}\cdot\hat{\boldsymbol{\beta}}_1$; (b) measured spectra of lasing light

用光纤偏振分束器(PBS)对输出激光进行偏振分离，调节 PC3 将 $\pm\hat{\boldsymbol{\beta}}_1$ 偏振模式的激光分别由 PBS 的 x 和 y 端口输出。测试中设置 I_{p0_edfa}=86 mW。图 8(a)给出了 $\hat{\boldsymbol{p}}_{in}\cdot\hat{\boldsymbol{\beta}}_1=1$ 时 x 端口偏振激光输出的干涉谱，3 dB 线宽约为 0.75 kHz。此时，从 PBS 的 y 端口检测到了激光输出(红色曲线)的干涉频谱，该输出主要是由 PBS 的消光比不够高导致的。由于设置的泵浦功率远大于系统的 I_{p0th}，因此 $\hat{\boldsymbol{p}}_{in}\cdot\hat{\boldsymbol{\beta}}_1=0$ 时，系统工作在退偏域，可同检测到 x 轴和 y 轴偏振方向皆有激光输出，测得两者的 3 dB 线宽皆约为 0.75 kHz，如图 8(b)所示。由此可见，线腔 PMF-BRFL 系统可以实现窄线宽随机激光输出。

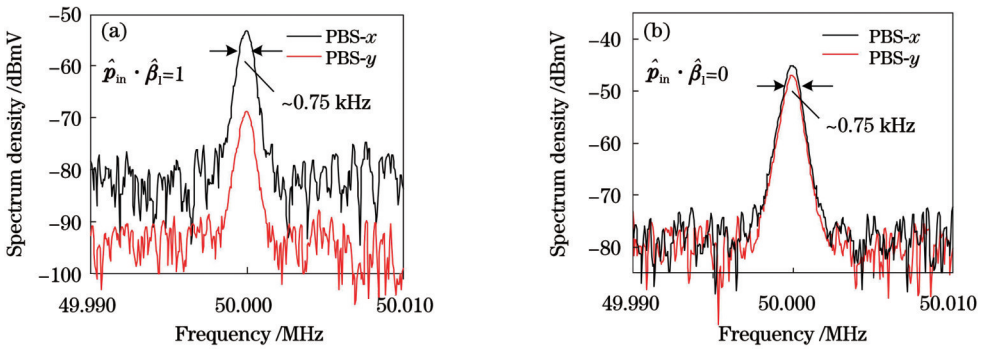

图 8　$\pm\hat{\boldsymbol{\beta}}_1$ 正交偏振模式下，PMF-BRFL 在 I_{p0_edfa}=86 mW、$\hat{\boldsymbol{p}}_{in}\cdot\hat{\boldsymbol{\beta}}_1$ 取值不同时激光输出线宽的测量曲线。(a) $\hat{\boldsymbol{p}}_{in}\cdot\hat{\boldsymbol{\beta}}_1=1$；(b) $\hat{\boldsymbol{p}}_{in}\cdot\hat{\boldsymbol{\beta}}_1=0$

Fig. 8　Measured linewidth curves of lasing light in $\pm\hat{\boldsymbol{\beta}}_1$ polarization modes for PMF-BRFL under conditions of I_{p0_edfa}=86 mW and $\hat{\boldsymbol{p}}_{in}\cdot\hat{\boldsymbol{\beta}}_1$ with different values. (a) $\hat{\boldsymbol{p}}_{in}\cdot\hat{\boldsymbol{\beta}}_1=1$; (b) $\hat{\boldsymbol{p}}_{in}\cdot\hat{\boldsymbol{\beta}}_1=0$

4　结　　论

笔者基于保偏光纤中 SBS 效应的轴向偏振牵引效应，提出并实现了一种正交偏振嵌位受激布里渊随机光纤激光器 PMF-BRFL。首先分析了 PMF 中的 SBS 增益与泵浦光、信号光偏振态之间的关系，结果显示，在 PMF-BRFL 中，PMF 主轴 $\pm\hat{\boldsymbol{\beta}}_1$ 偏振模式激光由于具有最大的 SBS 增益，能够胜出模式竞争在腔内振荡；接着推导出了 $\pm\hat{\boldsymbol{\beta}}_1$ 模式的激光振荡阈值条件，实现了对 PMF-BRFL 系统偏振模式工作区间的划分以及相应的工作条件的理论分析。采用 3 km 长 PMF 建立了 PMF-BRFL 系统，实验结果表明，PMF-BRFL 系统输出的随机激光偏振态可以稳定地嵌位于 $\pm\hat{\boldsymbol{\beta}}_1$ 偏振态上，具有良好的正交偏振嵌位整形能力。基于实验研究了泵浦功率及随机腔长对系统偏振嵌位工作范围的影响，并进一步研究了 PMF-BRFL 系统激光输出功率、输出光谱以及激光输出线宽的特性。本文提出的 PMF-BRFL 不仅可以实现偏振态稳定嵌位的窄带激光输出，还具有天然的输出激光偏振态的双稳态特性，在偏振控制、PolSK 通信、偏振整形及识别、偏振逻辑运算以及其他偏振双稳态相关应用中具有广阔的前景。

参　考　文　献

[1] Souidi Y, Taleb F, Zheng J B, et al. Low-noise and high-gain Brillouin optical amplifier for narrowband active optical filtering based on a pump-to-signal optoelectronic tracking[J]. Applied Optics, 2016, 55(2): 248-253.

[2] Chen Y, Lu Z W, Wang Y L, et al. Phase matching for noncollinear Brillouin amplification based on controlling of frequency shift of Stokes seed[J]. Optics Letters, 2014, 39(10): 3047-3049.

[3] Coles J B. Advanced phase modulation techniques for stimulated Brillouin scattering suppression in fiber optic parametric amplifiers [J]. Dissertations & Theses-Gradworks, 2016, 18(17): 18138-

18150.
[4] Casas-Bedoya A, Morrison B, Pagani M, et al. Tunable narrowband microwave photonic filter created by stimulated Brillouin scattering from a silicon nanowire[J]. Optics Letters, 2015, 40(17): 4154-4157.
[5] 田鑫, 王蒙, 王泽锋. 基于倾斜光纤 Bragg 光栅的受激布里渊散射滤波器[J]. 光学学报, 2020, 40(10): 1006002.
Tian X, Wang M, Wang Z F. Stimulated Brillouin scattering filters based on tilted fiber Bragg gratings[J]. Acta Optica Sinica, 2020, 40(10): 1006002.
[6] Morrison B, Marpaung D, Pant R, et al. Tunable microwave photonic notch filter using on-chip stimulated Brillouin scattering [J]. Optics Communications, 2014, 313: 85-89.
[7] 徐翌明, 潘炜, 卢冰, 等. 基于受激布里渊散射的多阻带微波光子滤波器[J]. 中国激光, 2018, 45(11): 1106004.
Xu Y M, Pan W, Lu B, et al. Multi-stopband microwave photonic filter based on stimulated Brillouin scattering[J]. Chinese Journal of Lasers, 2018, 45(11): 1106004.
[8] Sun A, Semenova Y, Farrell G, et al. BOTDR integrated with FBG sensor array for distributed strain measurement[J]. Electronics Letters, 2010, 46(1): 66-68.
[9] Jamioy C A G, Lopez-Higuera J M. Decimeter spatial resolution by using differential preexcitation BOTDA pulse technique[J]. IEEE Sensors Journal, 2011, 11(10): 2344-2348.
[10] Li W H, Bao X Y, Li Y, et al. Differential pulse-width pair BOTDA for high spatial resolution sensing[J]. Optics Express, 2008, 16(26): 21616-21625.
[11] 秦莉, 王澜澜, 梁浩, 等. 基于双边带干涉的预泵浦布里渊光时域分析系统[J]. 激光与光电子学进展, 2021, 58(1): 0106003.
Qin L, Wang L L, Liang H, et al. Pre-pump Brillouin optical time domain analysis system based on double-sideband interference[J]. Laser & Optoelectronics Progress, 2021, 58(1): 0106003.
[12] Zarinetchi F, Smith S P, Ezekiel S. Stimulated Brillouin fiber-optic laser gyroscope[J]. Optics Letters, 1991, 16(4): 229-231.
[13] Kadiwar R K, Giles I P. Optical fibre Brillouin ring laser gyroscope [J]. Electronics Letters, 1989, 25(25): 1729-1731.
[14] Fischer S, Meyrueis P, Schroeder W W. Brillouin backscattering in fiber optic gyroscope[J]. Proceedings of SPIE, 1995, 2510: 49-58.
[15] 杨茜, 周泽中, 刘恺, 等. 频率间隔可切换多波长布里渊随机光纤激光器[J]. 中国激光, 2022, 49(11): 1101003.
Yang Q, Zhou Z Z, Liu K, et al. Frequency interval switchable multi-wavelength Brillouin random fiber laser[J]. Chinese Journal of Lasers, 2022, 49(11): 1101003.
[16] 李亚方, 王春雨, 祁海峰, 等. 一种基于分布反馈光纤激光器的超窄线宽布里渊光纤激光器[J]. 激光与光电子学进展, 2020, 57(7): 071401.
Li Y F, Wang C Y, Qi H F, et al. An ultra-narrow linewidth Brillouin fiber laser based on distributed feedback fiber laser[J]. Laser & Optoelectronics Progress, 2020, 57(7): 071401.
[17] Song Y J, Zhan L, Ji J H, et al. Self-seeded multiwavelength Brillouin-erbium fiber laser[J]. Optics Letters, 2005, 30(5): 486-488.
[18] Saxena B, Ou Z H, Bao X Y, et al. Low frequency-noise random fiber laser with bidirectional SBS and Rayleigh feedback[J]. IEEE Photonics Technology Letters, 2015, 27(5): 490-493.
[19] Pang M, Bao X Y, Chen L. Observation of narrow linewidth spikes in the coherent Brillouin random fiber laser[J]. Optics Letters, 2013, 38(11): 1866-1868.
[20] Cao S, Zhang M. Polarized and birefringence-dependent stimulated Brillouin scattering in single mode fiber[J]. Optik, 2017, 131: 374-382.
[21] Shmilovitch Z, Primerov N, Zadok A, et al. Dual-pump push-pull polarization control using stimulated Brillouin scattering[J]. Optics Express, 2011, 19(27): 25873-25880.
[22] Zhang L, Xu Y P, Gao S, et al. Linearly polarized low-noise Brillouin random fiber laser[J]. Optics Letters, 2017, 42(4): 739-742.
[23] Wang L L, Dong X Y, Shum P P, et al. Random laser with multiphase-shifted Bragg grating in Er/Yb-codoped fiber[J]. Journal of Lightwave Technology, 2015, 33(1): 95-99.
[24] Smith A M. Birefringence induced by bends and twists in single-mode optical fiber[J]. Applied Optics, 1980, 19(15): 2606-2611.
[25] Galtarossa A, Palmieri L, Schiano M, et al. Statistical characterization of fiber random birefringence[J]. Optics Letters, 2000, 25(18): 1322-1324.
[26] Villafranca A, Lázaro J A, Salinas Í, et al. Stimulated Brillouin scattering gain profile characterization by interaction between two narrow-linewidth optical sources[J]. Optics Express, 2005, 13(19): 7336-7341.
[27] Ruffin A B, Li M J, Chen X, et al. Brillouin gain analysis for fibers with different refractive indices[J]. Optics Letters, 2005, 30(23): 3123-3125.
[28] Sugavanam S, Sorokina M, Churkin D V. Spectral correlations in a random distributed feedback fibre laser[J]. Nature Communications, 2017, 8: 15514.
[29] 巨海娟, 任立勇, 梁健, 等. 基于偏振控制技术提高光纤受激布里渊散射慢光稳定性研究[J]. 激光与光电子学进展, 2013, 50(3): 030603.
Ju H J, Ren L Y, Liang J, et al. Stability improvement of SBS slow light in optical fibers based on polarization management technique[J]. Laser & Optoelectronics Progress, 2013, 50(3): 030603.
[30] Ward B, Spring J. Finite element analysis of Brillouin gain in SBS-suppressing optical fibers with non-uniform acoustic velocity profiles[J]. Optics Express, 2009, 17(18): 15685-15699.
[31] Zadok A, Zilka E, Eyal A, et al. Vector analysis of stimulated Brillouin scattering amplification in standard single-mode fibers[J]. Optics Express, 2008, 16(26): 21692-21707.
[32] Wang C H, Zhang Q W, Mou C B, et al. Spectral polarization spreading behaviors in stimulated Brillouin scattering of fibers[J]. IEEE Photonics Journal, 2017, 9(1): 6100111.
[33] Wang C H, Zhang Y L, Liu G, et al. Orthogonal polarization switchable lasing based on axial polarization pulling of SBS in polarization-maintaining fiber[J]. Optics Express, 2018, 26(22): 28385-28395.

Brillouin Random Fiber Laser with Orthogonal Polarization Clamping

Ning Jinxing[1,2], Wang Chunhua[1,2*], Fang Nian[1,2], Gu Xiang[1,2], Wu Keshuai[1,2]

[1]*School of Communication and Information Engineering, Shanghai University, Shanghai* 200444, *China*;

[2]*Key Lab of Specialty Fiber Optics and Optical Access Networks, Shanghai University, Shanghai* 200444, *China*

Abstract

Objective The Brillouin random fiber laser (BRFL) is a new type based on stimulated Brillouin scattering (SBS) and a randomly distributed feedback resonator. Because SBS enables low-intensity noise, low-phase noise, and narrow-linewidth lasing light, it has

significant advantages in random fiber laser construction. However, research on BRFL has been limited to nonpolarization parameters, such as lasing power, intensity phase noise, and line width, rarely to polarization properties. In this study, a BRFL with a polarization-maintaining fiber (PMF) line-cavity (PMF-BRFL), in which lasering light with polarization clamped at either one of the two orthogonal principal axes of the PMF, is proposed and demonstrated based on the nonlinear axial polarization pulling effect of SBS in PMFs. A theoretical model of the PMF-BRFL is established, and the polarization properties of the lasing light related to the pump light and system parameters are analyzed, discussed, and compared with the experimental results, which were in good agreement with each other.

Methods First, based on the simplified polarization vector-propagation equations of SBS in PMFs, which theoretically indicate the axial polarization-pulling behavior of SBS in PMFs, we derived the analytical expression of the SBS gain in the PMFs, which presents the SBS gain expression to the input SOPs of the pump and signal light and the input pump power. Second, we derived lasing-pump power thresholds for the two polarization modes. We then analyzed the working conditions of these polarization regions. Furthermore, the width of the depolarization range W was analyzed, and its relationship with the pump power and cavity length was discussed.

The PMF-BRFL used a tunable laser to output the pump light with a center wavelength of 1553.73 nm, a polarization state generator (PSG) to generate 100-input SOPs of pump light with a relatively uniform distribution on the Poincaré sphere, an erbium-doped fiber amplifier (EDFA) to vary the input pump power, and a polarization controller to adjust the relative position of $\hat{\boldsymbol{p}}_{\mathrm{in}}$ to the principal axis of the PMF before the pump light entering a 3 km PMF fiber line-cavity via a normal single-mode fiber circulator (Cir). In a random cavity, the PMF acts as an SBS gain medium and provides the first and second Rayleigh scattering (RS) in opposite directions for random reflection. The SBS Stokes the light generated in the PMF emitted through Cir. At the PMF-BRFL output, the polarization behaviors, including Stokes parameters and degree of polarization, lasing power, optical spectrum, and linewidth of the lasing light, were measured using a polarization analyzer (PSA), an optical spectrum analyzer (OSA), and an electronic spectrum analyzer (ESA).

Results and Discussions When the cavity length increases from 1 to 5 km, the lasing threshold of the pump power at zero depolarization decreases from 75 to 29 mW, and the dynamics of the pump power for $W<0.1$ requirement decreases from 7 to 2.5 mW. For more extended cavities (5–11 km), $I_{\mathrm{p0th},W=0}$ decreases slightly, only from 29 to 21 mW, and the dynamics of the pump power for $W<0.1$ requirement remains almost unchanged around 2.5 mW (Fig. 2). Therefore, the cavity length of the established PMF-BRFL system can achieve an increased pumping efficiency by selecting a PMF of 3–5 km.

For different settings of power emitted from the EDFA, $I_{\mathrm{p0\_edfa}}=40$, 50, 55, 80, and 120 mW. As the input SOP of the pump light is scanned in the generated $\hat{\boldsymbol{p}}_{\mathrm{in}}^{\neq 100}$ pattern, almost all the SOPs of the lasing light clamp at either of the $\pm\hat{\boldsymbol{\beta}}_1$ positions and show a definite relationship of $\mathrm{sign}(\hat{\boldsymbol{p}}_{\mathrm{in}}\cdot\hat{\boldsymbol{\beta}}_1)\hat{\boldsymbol{\beta}}_1$, except for the cases for W of $\hat{\boldsymbol{p}}_{\mathrm{in}}\cdot\hat{\boldsymbol{\beta}}_1\approx 0$. For lasing lights clamped at $\pm\hat{\boldsymbol{\beta}}_1$ polarization, the system works in the full polarization regions, with measured DOP=1. However, for lasing lights with DOP<1, the system operates in the depolarization region, and both $\pm\hat{\boldsymbol{\beta}}_1$ modes oscillate simultaneously with different quantities, resulting in different DOPs observed inside the Poincaré sphere (Fig. 5).

W attains the lowest value at $I_{\mathrm{p0\_edfa}}=55$ mW, indicating $I_{\mathrm{p0th},W=0}$ of the PMF-BRFL with 3 km PMF is near 55 mW. At $I_{\mathrm{p0\_edfa}}=55$ mW, depolarization interval W is the narrowest, and the polarization clamping range of the system is the broadest. At $I_{\mathrm{p0\_edfa}}<55$ mW, a spontaneous region exists around $\hat{\boldsymbol{p}}_{\mathrm{in}}\cdot\hat{\boldsymbol{\beta}}_1\approx 0$, where PMF-BRFL emits weak and depolarized light. At $I_{\mathrm{p0\_edfa}}>55$ mW, the depolarization region also increases, and W increases with increasing pump power. The relationship between W and $I_{\mathrm{p0},W=0}$ of the PMF-BRFL was measured, and assuming that the Cir insert loss is 1.87 dB, the measured curve is consistent with the theoretical curve for a cavity length of 3 km (Fig. 6).

Moreover, the variation in the lasing power with $\hat{\boldsymbol{p}}_{\mathrm{in}}\cdot\hat{\boldsymbol{\beta}}_1$ was determined, and the spectra of the lasing light were measured for different $\hat{\boldsymbol{p}}_{\mathrm{in}}\cdot\hat{\boldsymbol{\beta}}_1$ values. The lasing power decreases with decreasing $\left|\hat{\boldsymbol{p}}_{\mathrm{in}}\cdot\hat{\boldsymbol{\beta}}_1\right|$, with a power difference of ~15 dBm between $\left|\hat{\boldsymbol{p}}_{\mathrm{in}}\cdot\hat{\boldsymbol{\beta}}_1\right|=1$ and 0 at the working point of $I_{\mathrm{p0\_edfa}}=55$ mW. Finally, the linewidths of the lasing lights in the two polarization modes are measured for $\left|\hat{\boldsymbol{p}}_{\mathrm{in}}\cdot\hat{\boldsymbol{\beta}}_1\right|=1$ and 0, and all lights have a narrow linewidth of ~0.75 kHz (Fig. 8).

Conclusions In this study, a BRFL with bistable orthogonal polarization was proposed and achieved based on the axial polarization pulling effect of the SBS effect in PMFs. First, the polarization mode working regions of the PMF-BRFL system and the corresponding working conditions were analyzed and discussed. In addition, a PMF-BRFL system was experimentally established using a 3 km PMF fiber. The laser can emit narrow-linewidth lasing light with a polarization state stably clamped onto one of the principal axes of the PMF, and the experimental results are consistent with the theoretical analysis. Furthermore, the effects of the pump power and cavity length on the working regions of the system and the characteristics of the lasing power, spectrum, and linewidth were investigated experimentally.

Key words lasers; stimulated Brillouin scattering; random fiber laser; polarization pulling effect; orthogonal polarization clamp; polarization maintaining fiber